Long-term durability of platelet-type carbon nanofibers for OER and ORR in highly alkaline media

Yuki Sato[†], Damian Kowalski[§]*, Yoshitaka Aoki[§], and Hiroki Habazaki[§]*

[†]Graduate School of Chemical Sciences and Engineering, Hokkaido University, Sapporo, Hokkaido 060-8628, Japan

[§]Division of Applied Chemistry, Faculty of Engineering, Hokkaido University, Sapporo, Hokkaido 060-8628, Japan

*Corresponding Author.

Tel: +81-11-706-6738. E-mail: kowalski@cat.hokudai.ac.jp (Damian Kowalski)

Tel: +81-11-706-6575. E-mail: habazaki@eng.hokudai.ac.jp (Hiroki Habazaki)

Keywords: platelet type carbon, electrocatalysis, zinc-air battery, oxygen evolution reaction

Graphical abstract

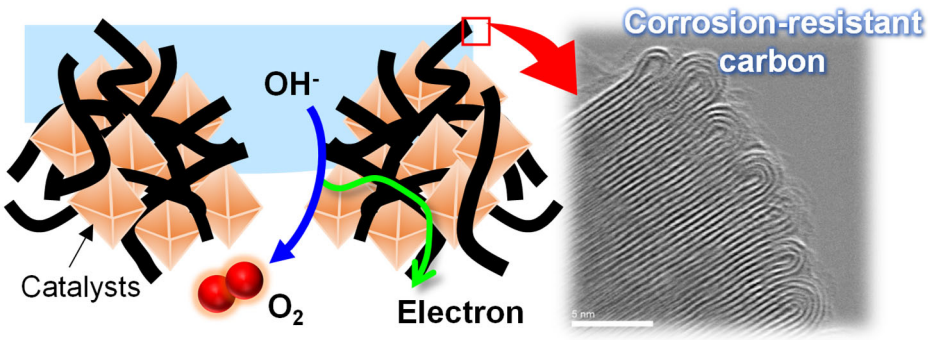

Highlights

· New carbon material having platelet structure

· Highly durable carbon nanofibers for OER/ORR in alkaline media

· High degree of graphitization and the slow oxidation rate of carbon edge planes

· Possibility of the graphitized platelet-type carbon nanofibers as the conductive supports for OER/ORR electrodes

Abstract

Highly durable air electrodes for the oxygen evolution reaction (OER) and oxygen reduction reaction (ORR) in highly alkaline media are necessary to catalyze reactions in metal-air secondary batteries. Carbon is able to provide electronic conductivity and co-catalyze reactions, however is typically oxidized under high-potential conditions above 1.1 V vs RHE. Herein, we demonstrate highly durable platelet-type carbon nanofibers (pCNFs) for OER/ORR in alkaline media. The pCNFs have graphene layers arranged perpendicularly to the fiber axis of the nanofibers. Such a specific configuration of the graphene layers in combination with a high degree of graphitization was found to be highly efficient in providing long-term durability combined with a state-of-the-art brownmillerite-type Ca_2FeCoO_5 catalyst. The improved oxidation resistance of the pCNF carbon is associated with the high degree of graphitization and the extremely slow oxidation rate of carbon edge planes at the sidewalls of the nanofibers.

1. Introduction

Metal-air secondary batteries (MABs) are promising candidates for the development of next-generation energy storage systems because of their relatively high theoretical energy density exceeding 1000 W h kg^{-1} [1]. An alkaline-aqueous electrolyte battery has advantages over organic electrolyte batteries, such as better safety and high ionic conductivity, resulting in easy energy output for the cell. The basic operation of the positive electrode is directly linked to the kinetics of the oxygen evolution reaction (OER) and oxygen reduction reaction (ORR) taking place during the charging and discharging processes, respectively. To promote both reactions, a reversible air electrode possessing high durability for the repeated charging/discharging in addition to a high electrocatalytic activity for OER and ORR is necessary. The state-of-the-art electrocatalysts for OER are typically composed of precious metals such as RuO_2 and IrO_2 [2, 3], and Pt/C hybrids are used for ORR [4]. The development of new oxide catalysts containing earth-abundant elements is in high demand to lower the costs of MABs [5-9]. Very recently, our group reported a very high OER activity of the brownmillerite-type oxide Ca_2FeCoO_5 (CFCO) [10-12]. The general shortcoming for this type of electrocatalyst is its moderate charge transfer characteristics [13] together with poor ORR electrocatalytic activity, where good activity is necessary for MAB operation [14, 15]. Modification of the electrocatalyst with carbon materials is one of the possible approaches commonly used for perovskites to overcome conductivity issues. Carbon is a well-known and promising conductive material due to its good electrochemical characteristics, its lightweight and earth-abundant characteristics, and its role as a cocatalyst for ORR [1,16-18]. Thus, carbon materials can be considered as conductive supports for metal oxide electrodes for metal-air secondary batteries such as CFCO.

The operation of an air-positive electrode in an alkaline metal-air battery is based on OER and ORR via the following scheme:

$$O_2 + 2H_2O + 4e^- \rightleftarrows 4OH^- \qquad E^0 = 1.23 \text{ V vs RHE} \qquad (1)$$

The four-electron reaction pathway described in (1) leads to the presence of a relatively large

overpotential in electrochemical terms [19]. Under these electrochemical conditions, however, carbon is easily oxidized in highly alkaline media through two elementary steps via the following reactions [16, 19-22]:

$$C + 4OH^- \rightarrow CO_2 + 2H_2O + 4e^- \quad (2)$$

$$CO_2 + 2OH^- \rightarrow CO_3^{2-} + H_2O \quad (3)$$

or, alternatively, by a one-step reaction, with the standard electrode potential established at 1.01 V vs RHE [20].

$$C + 6OH^- \rightarrow CO_3^{2-} + 3H_2O + 4e^- \quad (4)$$

By looking at the Pourbaix diagram, one may find a very narrow potential-pH window at which the carbon would be thermodynamically stable [21, 22]. The harsh operating conditions for metal-air-batteries, *i.e.*, working potentials outside of the thermodynamic stability of water and pH ≥ 13, lead to oxidation of carbon during the charging process. Therefore, good oxidation resistance of the carbon supports is one of the critical aspects to improve the durability of metal-air batteries, and new carbon materials with oxidation resistance capability are thus highly desirable. There is a growing body of literature that suggests requirements for durable carbon materials for electrochemical oxidation. The graphitization degree has been found to influence the oxidation resistance of carbon studied by electrochemical measurements combined with liquid/gas chromatography, as well as mass spectrometry [23]. It was demonstrated that highly graphitized carbon has a lower corrosion rate than that of a material with a low graphitization degree due to its highly ordered stable structure. Moreover, an edge plane of a graphite crystal is considered to be much more reactive than a basal plane [24-27]; thus, such edge sites may be the priority sites for oxidation.

Taking into account the above reports, the proper design of carbon structures such as the combination of highly graphitized carbon with elimination of the exposure of carbon edge planes may provide oxidation resistance not achievable by classic carbon materials. Herein, our focus is on platelet-type carbon nanofibers (pCNFs) with a graphene layered structure with exposed functional

graphene edges on the sidewalls. These edges have already been reported to be highly active sites on the carbon surface during the nanoparticle deposition process in the liquid phase [28, 29]. The pCNFs with a graphene layered structure and exposed edges facilitated lithiation/delithiation when applied as a negative electrode in Li-ion batteries, thereby increasing the charge storage capacity to 372 mA h g^{-1} [30]. Li et al. demonstrated that graphene edges play the role of active sites during ORR, which is the key reaction for the operation of positive electrodes in metal-air batteries [27]. Such graphene edge sites can be considered easily degradable under oxidizing conditions and therefore cause carbon oxidation. The surface of pCNFs may be effectively controlled by means of thermal treatment because the structure is dynamically changed with the applied temperature [31-34]. Our group reported that the exposed edge forms a loop structure when pCNFs are heat-treated at temperatures higher than 2000°C [31]. The heat-treated pCNFs are characterized by a high degree of graphitization and have eliminated the exposed carbon edges by means of loop formation. Both features may be suitable for designing electrocatalyst carbon supports with high corrosion resistance for use in oxygen evolution reactions. In the present study, we combine the brownmillerite-type electrocatalyst with pCNFs heat-treated at 1500 and 2400°C to investigate the relationship between structural changes and electrocatalytic activity towards OER/ORR as well as the durability.

2. Experimental

2.1 Preparation of the AAO template and pCNFs

The pCNFs were prepared by liquid-phase carbonization in a porous anodic alumina template according to a procedure described elsewhere [31]. Briefly, a template of porous anodic alumina (AAO) films was prepared by anodizing 99.99% pure aluminum sheets (10 x 10 cm^2, thickness 0.1 mm) at 40 V in 0.3 mol dm^{-3} oxalic acid aqueous solution at 20°C for 2 h. The size of the nanopores in the anodic alumina layer was controlled by subsequent pore widening treatment in 5 wt% H_3PO_4 for 30 min at 30°C. Under these conditions, the thickness of the AAO template and the pore size were controlled at approximately 16 μm and 50 nm, respectively (Fig. S1). Polyvinyl chloride powders (PVC, SHIN-ETSU CHEMICAL Co., Ltd., TK-2500) were used as a carbon precursor. The AAO template and PVC powders were mixed and heat-treated first at 300°C for 30 min with a temperature ramp of 400 K h^{-1} in a stream of high-purity argon (99.999%) followed by heat treatment at 600°C for 1 h. The PVC was converted to a liquefied intermediate at ~300°C, penetrating into the pore channels of the template. The template was then dissolved in 10% NaOH solution under ultrasonication, and the pCNFs were filtered. Further heat treatment was performed at 1500 or 2400°C, and the pCNFs were consequently denoted as pCNF1500 and pCNF2400, respectively. The preparation process is illustrated in Fig. S1.

2.2 Synthesis of CFCO

CFCO electrocatalyst was synthesized according to a procedure described elsewhere [10]. The following reagents were used as precursors: $Ca(NO_3)_2 \cdot 4H_2O$ (Kanto Chemical, 99.9%), $Fe(NO_3)3 \cdot 9H_2O$ (Kanto Chemical, 99.9%) and $Co(NO_3)_2 \cdot 6H_2O$ (99.9%, Wako Pure Chemical). Appropriate amounts of these reagents were dissolved in Milli-Q water in which an equimolar amount of citric acid (Wako Pure Chemical, 98%) was subsequently added as a complexing agent. The citrate solution was stirred and heated at 60 - 70°C to promote polymerization. The gelatinous product was prefired in air at 450°C for 1 h and then fired at 600°C for 12 h.

2.3 Characterizations

The phase purities and the graphitization degrees of the carbon materials used in this study were examined by X-ray powder diffraction (XRD; Rigaku, Ultima IV) using Cu Kα radiation ($\lambda = 0.15418$ nm) operated at 40 kV and 20 mA. The graphitization degree was also examined by Raman spectroscopy (Horiba Scientific, XploRA) using a 532 nm laser beam. The detailed structure was further evaluated using transmission electron microscopy (TEM; JEOL, JEM-2000FX, JEM-2010F and JEM-ARM200F) with the system operated at 200 kV. The surface morphology was observed by using a low-voltage scanning electron microscope (Zeiss, Sigma-500) operated at 1.5 kV. To estimate the BET surface areas, nitrogen gas adsorption/desorption isotherm measurements (Bel Japan, Belsorp-mini instrument) were conducted at -196°C.

2.4 Electrochemical measurements

In this work, the following carbon materials were used as conductive supports: pCNF1500, pCNF2400, Denka black (DB, Denka Ltd.), Denka black heat-treated at 2400°C (DB2400) and multiwalled carbon nanotubes (MWCNTs, Sigma Aldrich, PR-25-XT-HHT). Denka black was heat-treated under the same conditions as those of pCNF2400. Ten milligrams of selected carbon and 50 mg of CFCO were dispersed ultrasonically in a mixture of 0.2 mL of 5 wt% Na^+-exchanged Nafion solution and 4.8 mL of ethanol to obtain a catalyst ink. Nafion was added as a binder and neutralized before dispersion to prevent CFCO from undergoing acidic dissolution due to the lower pH of the Nafion binder [35]. The catalyst ink was loaded onto a glassy carbon electrode, and the loaded catalyst amount was 1.0 mg cm^{-2}. The evaluation of electrocatalytic activity was performed by means of linear sweep voltammetry (LSV) using a rotating disk electrode (RDE) at 1600 rpm with a potential sweep rate of 1 mV s^{-1}. The durability tests were performed on PTFE-coated carbon sheets (ElectroChem, Inc., EC-TP1-060T), on which the total catalyst mass of 1.0 mg cm^{-2} was loaded on each electrode. The electrochemical measurements were carried out in a three-electrode system using a Princeton Applied Research VersaSTAT3 potentiostat. A carbon sheet and Hg/HgO/4 mol dm^{-3} KOH with O_2 saturation were used as counter and reference electrodes, respectively. All measurements were carried out at room temperature (~25°C) in a 4 mol dm^{-3} KOH aqueous solution (pH = 14). The potential U was converted from the Hg/HgO/4 mol dm^{-3} KOH reference scale to the RHE using the following equation [10]:

$$U \text{ vs RHE} = U \text{ vs Hg/HgO/4 mol dm}^{-3} \text{ KOH} + 0.098 + 0.059 \times \text{pH} \quad (5)$$

The calculated position on the RHE potential scale was in agreement with the potential measured directly with a commercial reversible hydrogen electrode (ET070 HydroFlex, Gaskatel). The durability tests were continuously carried out for each carbon/CFCO electrode for a maximum of 1 month, in which cycles of 2 h chronopotentiometry at +40 mA cm^{-2} and subsequent 15 min rest mode at open-circuit potential (OCP) were repeated for 1 month in a 4 mol dm^{-3} KOH electrolyte.

Electrochemical impedance spectroscopy (EIS) was also used to characterize the electrode. The measurements were performed at a constant potential of 1.6 V vs RHE in 4 mol dm^{-3} KOH electrolyte with the amplitude of the AC perturbation signal at 10 mV in the frequency range from 10^{5} Hz to 10^{-2} Hz.

3. Results and Discussion

3.1 Materials characterization

The three main types of carbon structures used in this study are schematically illustrated in Fig. 1. Type 1 (pCNF1500, pCNF2400) refers to a structure with graphene layers arranged perpendicularly to the fiber axis of the nanofiber, type 2 (MWCNT) is a structure with graphene layers parallel to the fiber axis of the nanofiber, and type 3 (DB, DB2400) is a stack of particles with graphene layers randomly distributed along each particle. The exposed surface of pCNF1500 consists mainly of the carbon edge plane, whereas the carbon basal plane is exposed for pCNF2400, MWCNTs and DB. The carbon edge side typically contains dangling bonds, sp^3 sites, and functional groups leading to edge reconstruction, passivation or termination. Consequently, a higher number of defect sites is expected on the edge plane than on the basal plane, which act as hosts for molecules to adsorb, especially for gas species altering the electrochemistry of the carbon [36, 37].

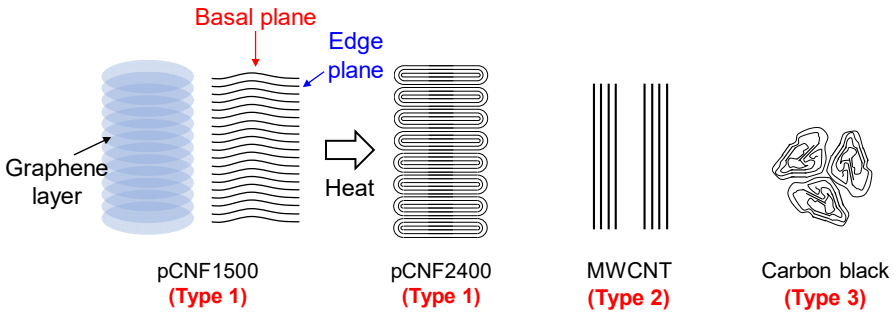

Fig. 1 Schematic illustration of the carbon materials used in this study.

The SEM images of the above carbon materials are shown in Fig. 2. The samples pCNF1500 (Fig. 2a) and pCNF2400 (Fig. 2b) possess a nanofiber morphology with an average diameter of 50 ± 8 nm, which agrees with the pore size of the anodic alumina (AAO) template (Fig. S1). The length of the pCNFs was less than 2 μm, which was much shorter than the length of the cylindrical pore channel (16 μm) in the template. The formation of short nanofibers was associated with the trapping of gaseous species generated during carbonization of the PVC precursor in the cylindrical pores of the AAO template as well as the poor mechanical strength of platelet-type CNFs [30, 31]. The above morphological characteristics did not appear to be changed by means of heat treatment temperature at the available SEM resolution. The commercial MWCNTs used in this study (Fig. 2c) had lengths in the range of 0.5 – 10 μm with a diameter of 50–200 nm, possessing an aspect ratio larger than that of the pCNFs by a factor of 2. DB, a commercial type of acetylene black, and the DB annealed at 2400°C (DB2400) show a nanoparticle-type morphology with a particle size of 40 ± 10 nm. No morphological changes such as agglomeration and/or particle shrinking were observed upon heat treatment.

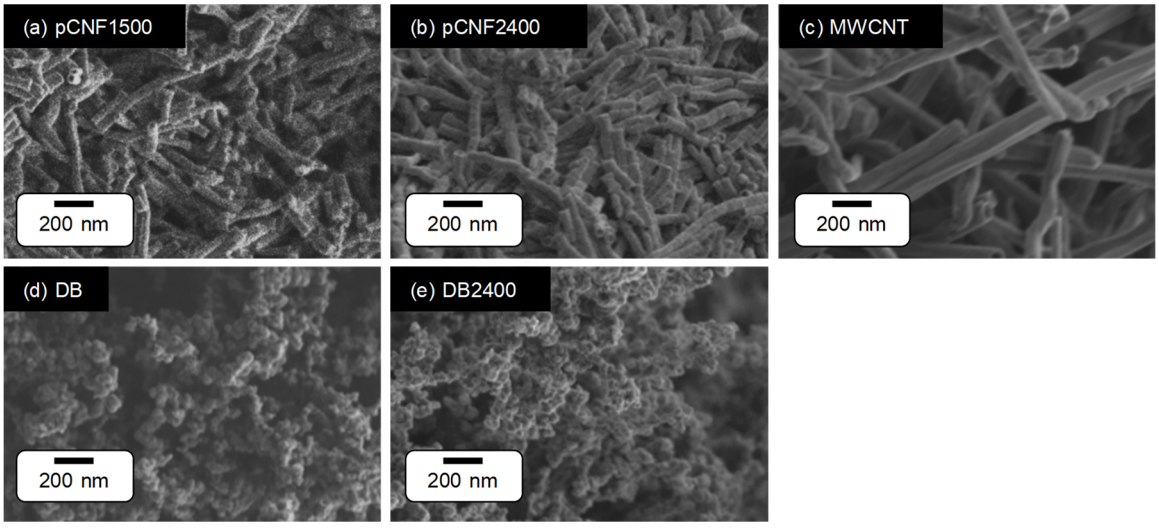

Fig. 2 SEM images of (a) pCNF1500, (b) pCNF2400, (c) MWCNT, (d) DB and (e) DB2400 carbon materials.

The detailed carbon structure was further investigated by TEM. Figure 3a and 3b shows that pCNF1500 and pCNF2400 (type 1) have platelet structures with graphene layers perpendicularly oriented to the fiber axis of the nanofibers. The graphene structure is established by the specific interaction between the AAO template and the polycyclic aromatic intermediates compound formed during thermal decomposition of PVC [38]. One of the most noticeable differences between pCNF1500 and pCNF2400 is the formation of looped graphene edges for pCNF2400, with most regular loops formed after treatment at 2400°C. Each loop contains 3-5 graphene layers; therefore, each stack is composed of 6-10 graphene layers. The lattice fringes for pCNF2400 were more developed than those of pCNF1500. Figure 3c shows the TEM image for a MWCNT (type 2), in which the carbon layers are oriented parallel to the fiber-axis of the nanotube. In this configuration, the basal planes of carbon were predominantly exposed at the sidewalls of the MWCNTs. In the case of the type 3 structures studied for DB (Fig. 3d) and DB2400 (Fig. 3e), the carbon basal planes were mainly exposed on the surface. The lattice fringes were incompletely developed for type 3 nanostructures even for DB2400, and therefore, random regions were formed on the carbon particles. The randomly distributed domains remained unmodified after heat treatment at 2400°C. The growth of the platelet structure and increasing graphitization degree with heat treatment temperature are apparent from the above TEM observations of type 1 carbon. Furthermore, the disordered carbon structure of DB is maintained even after heat treatment above 2000°C.

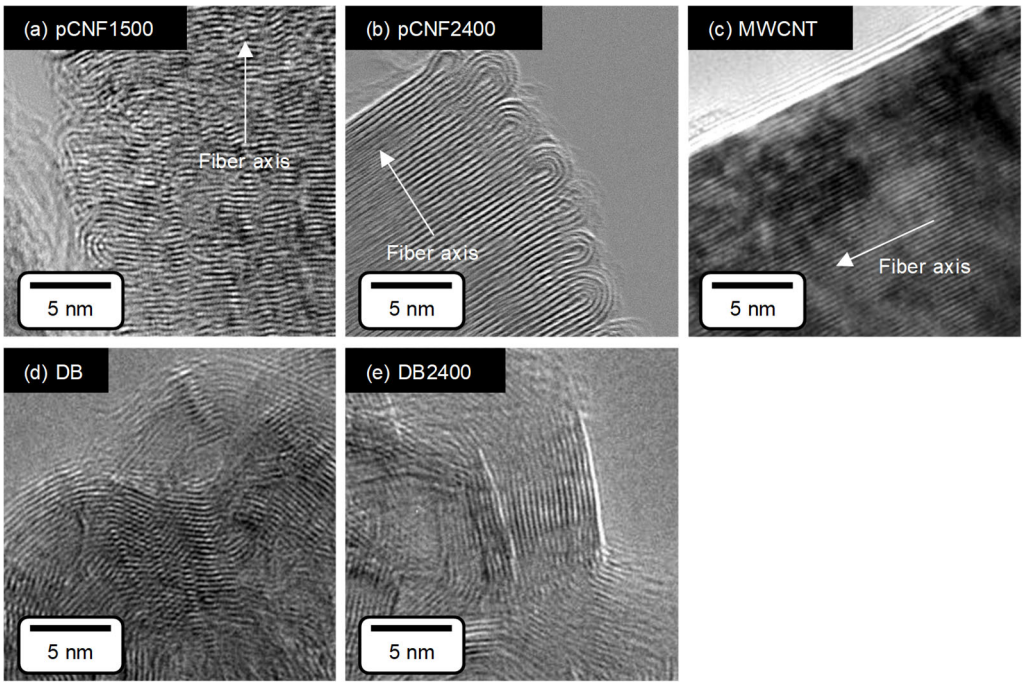

Fig. 3 HRTEM images of (a) pCNF1500, (b) pCNF2400, (c) DB and (d) DB2400 and (e) MWCNT carbon materials.

Figure 4 shows the X-ray diffraction (XRD) patterns and Raman spectra of the carbon materials. The XRD patterns (Fig. 4a) show the presence of 2θ diffraction angles at 25°, 42°, and 54° corresponding to the carbon 002, 10, and 004 reflections, respectively. The 002 peak becomes narrower for pCNFs with increasing heat treatment temperature, whereas a broad peak is observed for DB and DB2400. One may also notice that with increasing heat treatment temperature, the peak position shifts towards higher angles, from 25.6° for pCNF1500 to 26.2° for pCNF2400, indicating an increase in the graphitization degree. The above results also reveal that the pCNFs heat-treated at 2400°C have a higher graphitization degree. The enhancement of the graphitization degree for pCNF2400 is clearly visible if one compares DB2400 with pCNF2400. The full width at half maximum (FWHM) of the 002 peak for DB changed from 1.24° to 1.09° after heat treatment at 2400°C, although there was no peak shift after the heat treatment for DB.

To estimate the graphitization degree, the interplanar spacings, d_{002}, and crystalline domain size (L_C) were calculated according to equations (6) and (7),

$$d_{002} = \frac{\lambda}{2\sin\theta} \quad (6)$$

$$L_{c,002} = \frac{\mathrm{K}\lambda}{\beta\cos\theta} \quad (7)$$

where λ, K and β are the X-ray wavelength (0.15418 nm), the shape factor (K = 0.9) and FWHM of the C 002 peak, respectively. The values of d_{002}, summarized in Table 1, indicate that the interlayer spacing gradually decreases with increasing heat treatment temperature, reaching a d_{002} value close to that of the ideal graphite structure (0.3354 nm). The crystallite size, L_c, calculated from the Scherrer equation, increases with heat treatment temperature. Considering the XRD characteristics, MWCNTs have the highest graphitization degree among the other carbon materials, which is comparable with that of pCNF2400.

The graphitization degree was also investigated by means of Raman spectroscopy (Fig. 4b). In the Raman spectra, the E_{2g} vibration mode of graphite is attributed to the stretching vibration in the aromatic layers and occurs at a frequency of approximately 1580 cm^{-1} [39]. This mode is generally referred to as the G band. In the investigated frequency range, the G band is the only band that appears in a perfect graphite structure. Additional bands may also be found at approximately 1350, 1500, and 1620 cm^{-1} for less ordered carbon materials. The 1350 cm^{-1} band, known as the defect band (D band), is typically assigned to the A_{1g} mode or to the breakdown of transitional and local lattice symmetries [40-42]. The Raman spectra for pCNF1500 and DB presented in Fig. 4b show two broad overlapping bands located at ~1580 cm^{-1} (G band) and ~1350 cm^{-1} (D band). With the increase in the thermal treatment temperature up to 2400°C, both bands become narrower, their intensities increase, and the maxima move towards lower wavenumbers, which is expected since the defects present in the pristine material are eliminated upon heat treatment. An additional signal was found at ~1620 cm^{-1} for pCNF2400 corresponding to the D' band. The position and width of the D and G bands may serve as

indicators for the graphitization degree [43], which is often calculated by comparing the intensity ratio for the D and G bands using the following formula: graphitization degree = I_D/I_G [44], where I_D and I_G represent the peak area of the D band (1350 cm^{-1}) and G band (1580 cm^{-1}), respectively. The results are summarized in Table 1. There is a significant improvement in the structural organization of the type 1 carbon materials observed with the increased heat treatment temperature, but the organization is limited for the type 3 carbon materials.

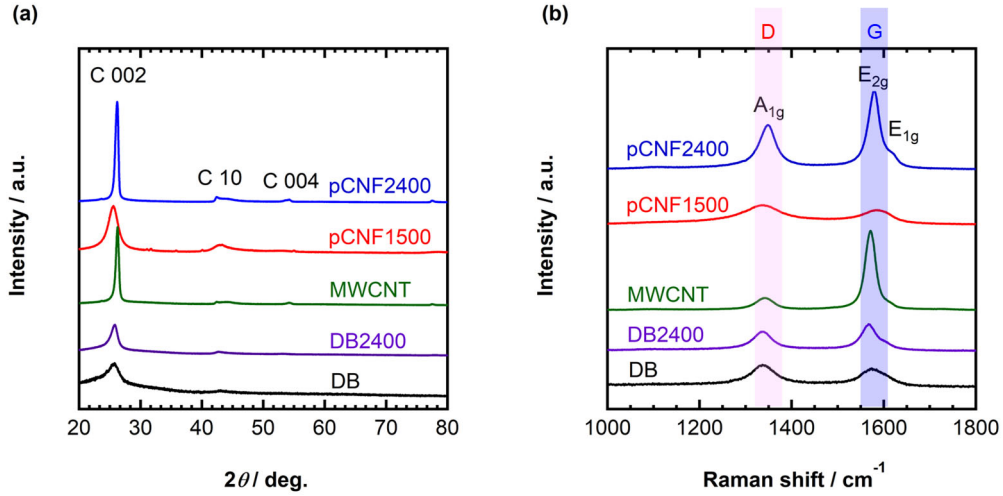

Fig. 4 (a) XRD patterns and (b) Raman spectra of carbon materials used in this study.

Table 1 Structural characteristics of carbon materials used in this study.

	d(002) / nm	*Lc* / nm	Raman I_D/I_G	BET / m^2 g^{-1}	Average diameter or particle size / nm
pCNF1500	0.348	5.0	1.64	32.0	50
pCNF2400	0.340	14	0.698	28.0	50
MWCNT	0.339	16	0.193	72.1	50-200
DB	0.346	7.1	0.938	59.4	40
DB2400	0.345	8.1	0.832	42.7	43

Figure S2 shows nitrogen gas adsorption/desorption isotherms for the carbon materials. The isotherms suggested the presence of limited amounts of micropores and mesopores. The BET surface areas estimated using the adsorption isotherms of Fig. S2 are summarized in Table 1. The influence of heat treatment on the BET surface areas is relatively small for the type 1 and type 3 carbon materials. pCNF-type carbon materials have the lowest BET surface areas among the carbon materials examined and approximately half that of MWCNTs.

3.2 OER activity and durability

CFCO is an efficient electrocatalyst for OER in highly alkaline media [10-12]. Herein, we tested each carbon material as a conductive support for CFCO for OER. Figure 5a shows linear sweep voltammograms for carbon supports/CFCO, demonstrating catalytic activity towards OER in 4 mol dm^{-3} KOH. The overpotential at high current densities was reduced in the following order: DB2400/CFCO = DB/CFCO ≤ pCNF1500/CFCO ≤ pCNF2400/CFCO < MWCNT/CFCO << pristine-CFCO. The onset potential (E_{onset}), determined at a current density of 1.5 mA cm^{-2}, for the OER for each carbon/CFCO composite electrode is 1.47 V vs RHE. In contrast to that of the carbon composite materials, E_{onset} for pristine Ca_2FeCoO_5 (without carbon support) is shifted towards a higher potential value of 1.50 V, indicating that the carbon support is necessary to promote OER for the brownmillerite-type CFCO electrocatalyst. The high current density tail in the LSV curve for pCNF2400/CFCO is shifted towards higher potential values with respect to those of pCNF1500- and DB-based electrocatalysts. The possible explanation for the shift is the insufficient dispersion of carbon material within the electrocatalyst matrix. Figures 5b and 5c show SEM-Backscattered-Electron (BSE) images for DB/CFCO and pCNF2400/CFCO, where the carbon materials and CFCO appear as dark and bright domains, respectively, due to the atomic number contrast. In the case of pCNF2400/CFCO, the agglomeration of pCNF2400 is visible as the large darker region. The better distribution of carbon in the DB/CFCO composite is apparent since much as smaller light regions (CFCO) and darker regions

(DB) are present. It is worth noting that the better distribution of carbon material within the composite matrix facilitates electron transfer for the electrocatalyst. The electrochemical characteristics of the catalyst under OER conditions were investigated by means of electrochemical impedance spectroscopy (EIS) measurements at a constant potential of 1.6 V vs RHE in 4 mol dm^{-3} KOH electrolyte (Fig. 5d). The Nyquist plots for DB/CFCO and pCNF2400/CFCO catalysts deposited on GC electrodes are shown for comparison. The impedance spectrum for pCNF2400/CFCO is characterized by two time constants; the high-frequency arc is associated with the resistance of the catalyst, whereas the low-frequency arc corresponds to charge transfer resistance, both having well-defined intersections at 0.5 kHz. Two-component impedance spectra, with one component associated with a metal oxide catalyst and the second corresponding to a charge transfer reaction, are typically observed for many other carbon/metal oxide catalysts [45, 46]. In contrast, the Nyquist plot of DB/CFCO is characterized by one semicircle, which is supposed to be a result of similar time constants for the charge transfer reaction and DB/CFCO component. It is obvious from Fig. 5d that the DB/CFCO electrode with better carbon dispersion shows a smaller charge transfer resistance than that of the pCNF2400/CFCO electrode with agglomerated carbon.

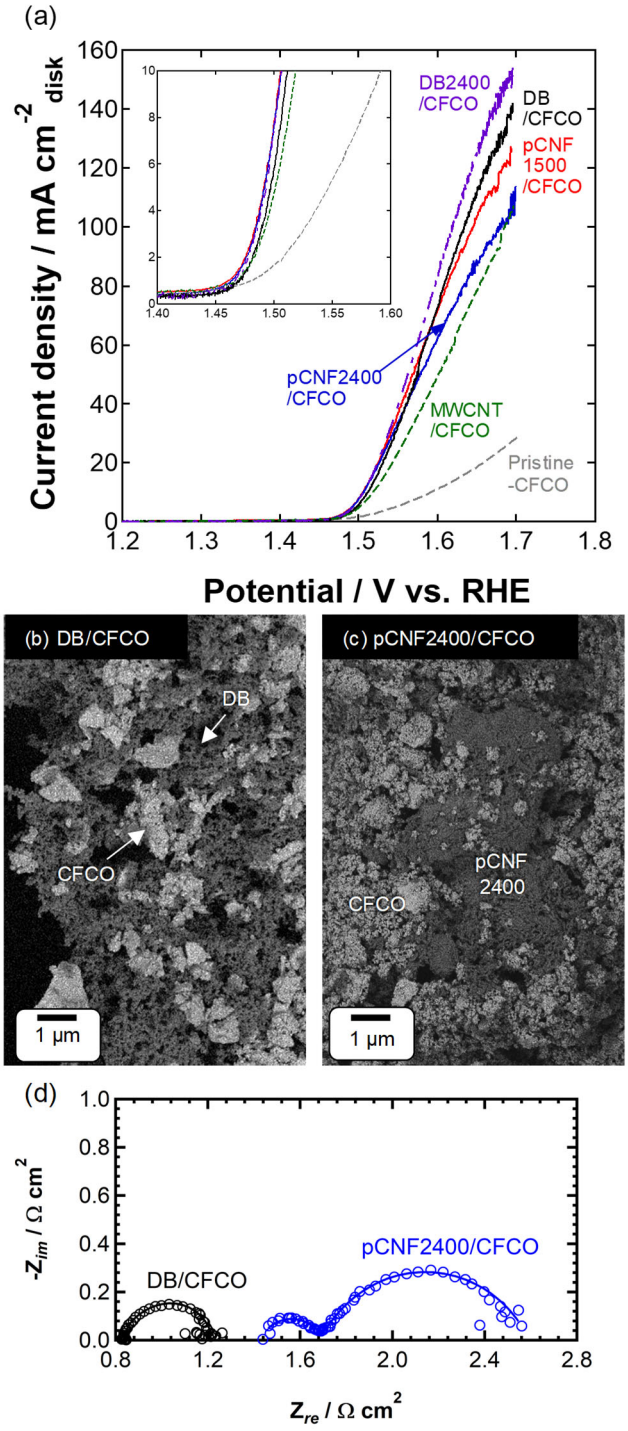

Fig. 5 (a) Linear sweep voltammograms of the carbon/CFCO electrodes for OER in 4 mol dm^{-3} KOH aqueous solution. The current density was normalized by the geometric surface area of the disk electrode; (b, c) SEM-BSE images of (b) DB/CFCO and (c) pCNF2400/CFCO electrodes on a GC substrate; (d) EIS Nyquist plots of DB/CFCO and pCNF2400/CFCO electrodes at 1.6 V vs RHE.

The long-term durability of carbon/CFCO electrodes under OER conditions was investigated by means of polarization at +40 mA cm^{-2} in 4 mol dm^{-3} KOH. Figures 6a and 6b show the anodic LSV curves for the carbon/CFCO electrodes before and after 14 days of polarization. The electrocatalytic activity of DB/CFCO, DB2400/CFCO and pCNF1500/CFCO towards OER was significantly reduced, with the current density at 1.7 V vs RHE dropping to 53%, 54% and 67% of the original value, respectively. The deactivation of the catalyst is possibly caused by oxidative decomposition of the carbon support and therefore the deficiency of electron-conducting paths to CFCO. A similar decrease in the OER current for perovskite oxide/carbon electrodes, related to carbon corrosion, was reported elsewhere [47]. The MWCNT/CFCO electrode showed deactivation towards OER with the current density dropping to 87% at 1.7 V vs RHE, but this performance decrease was slightly smaller than that with other carbons due to this sample having the highest graphitization degree and therefore better oxidation resistance. The electrocatalytic activity of pCNF2400/CFCO towards OER essentially remained unchanged under the same conditions for a period of one month. The origin of the high durability is likely associated with the structure of pCNF2400, which has high graphitization degree and eliminated graphene edges. Figure 6c shows the cathodic linear scanning voltammetry (LSV) curves obtained for the pCNF2400/CFCO electrode under a long-term durability test in oxygen-saturated 4 mol dm^{-3} KOH. The voltammogram was obtained by running the LSV experiment while the durability test cycles were in the rest mode. It is found that the ORR current gradually increases during the durability test. It is generally accepted that the ORR electrocatalytic activity of carbon/perovskites is linked to a synergistic effect between carbon and the metal oxide [1, 16-18]. The enhancement of catalytic activity for the oxidized carbon material has been observed by other researchers [48-50]. Herein, the enhancement of the ORR activity is most likely related to the partial oxidation of pCNF2400, without any significant effect on the OER activity. One of the possible explanations for the change in the ORR activity could be the stronger affinity of the oxygen molecules to adsorb on the edge sites compared to the plane sites [27, 36]. Density functional theory (DFT)

calculations have shown that dangling bonds at the edge sites of graphene have a strong ability for O_2 adsorption [36]. The slow ORR kinetics for pristine pCNF2400 would therefore be linked to the presence of loop sides on the fiber surface with exposed basal plane. The transformation of loops into edges under the long-term durability test increases the ORR kinetics as O_2 adsorption on the edge plane becomes more favorable.

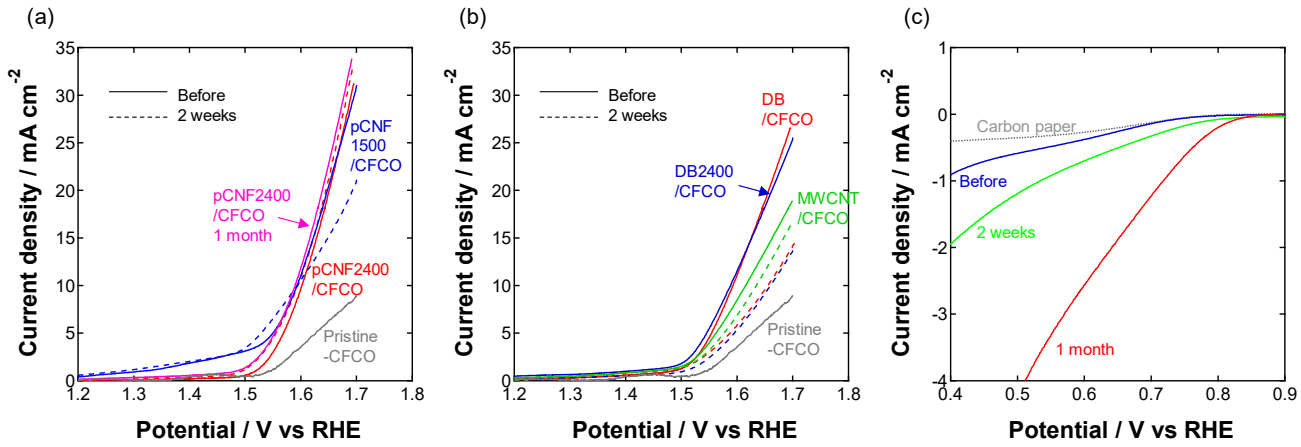

Fig. 6 Linear sweep voltammograms of carbon/CFCO electrodes for (a, b) OER and (c) ORR for pCNF2400/CFCO in 4 mol dm^{-3} KOH aqueous solution before and after the durability tests. The current density was normalized by the geometric surface area of the carbon paper electrode.

The morphological changes associated with carbon corrosion after a two-week durability test were observed by SEM-BSE observations. The results are shown in Fig. 7 and Fig. S3. After the durability test, the dark particles are absent for the pCNF1500/CFCO and DB/CFCO electrodes; only the substrate and/or Nafion binder film is visible due to the loss of carbon caused by the oxidative decomposition. Upon polarization of the specimen, the morphology of CFCO particles changes from a particle-like shape into a plate-like shape. This effect may be related to the *in situ* chemical change of CFCO to oxyhydroxide. A similar phenomenon was reported by other researchers [51-55], and we discussed this effect more in detail elsewhere [11, 12]. The other carbon materials, such as DB annealed at 2400°C and the highly graphitized MWCNTs, show a similar tendency regarding the surface morphology. In contrast, no morphological changes were observed for the pCNF2400/CFCO electrodes under the durability test. The pCNF nanofibers sustained their geometrical shape, and no exposed Nafion binders were observed, indicating that pCNF2400 is durable under OER conditions. Figure S4 shows TEM images before and after the durability test for MWCNT/CFCO. After the durability test, the MWCNT is partially corroded, with a reduced tube diameter. The TEM observations suggest that the oxidation proceeds locally and perpendicularly to the fiber axis of MWCNTs, with a pit-like morphology. In other words, the corrosion of MWCNTs occurs from the basal plane of carbon. The localized attack of graphitic carbon has been reported previously [56, 57]. The local oxidation may be associated with the presence of some structural defects in the basal planes, as reported previously [58].

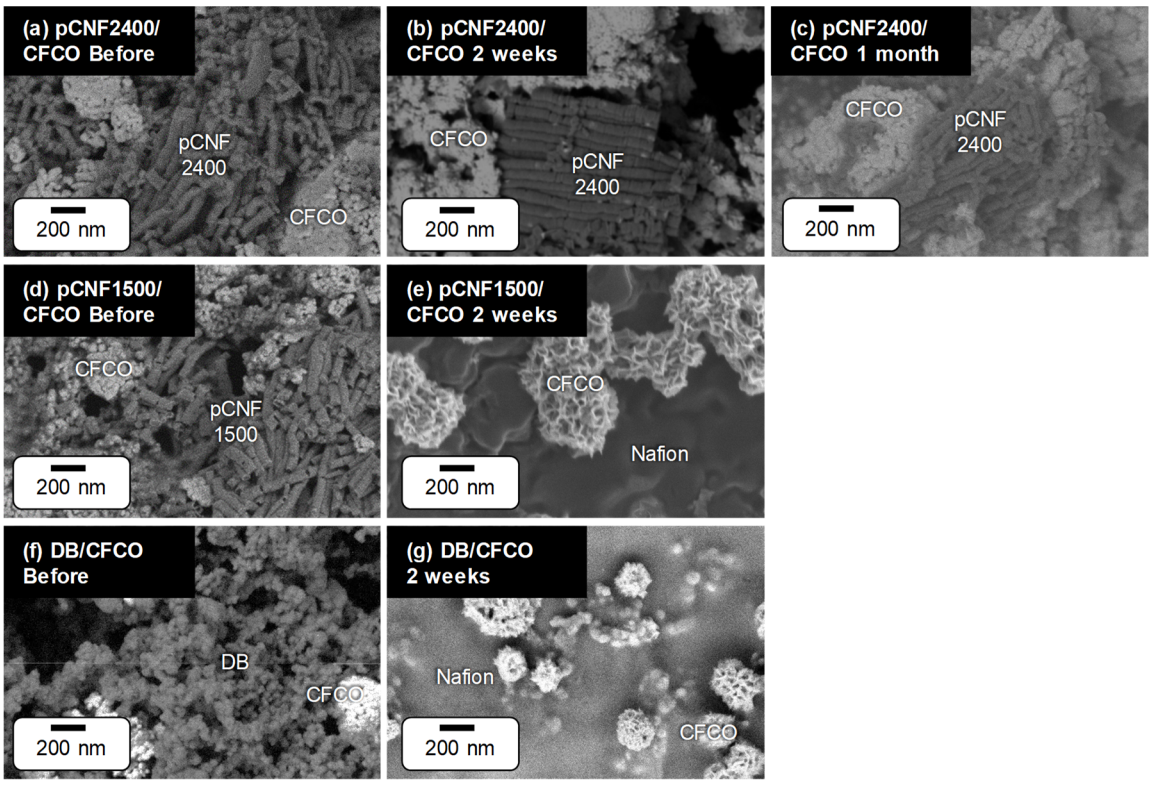

Fig. 7 SEM-BSE images of carbon/CFCO electrodes before and after the durability test for 2 weeks and 1 month.

The TEM images for pCNF2400 before and after the durability test are shown in Figs. 8 and S5. Fig. S5 reveals that the nanofiber diameters of pCNF2400 remained almost unchanged even after the durability test for 1 month. However, high-magnification images (Fig. 8) reveal the change in the structure of the sidewall of pCNF2400. Before the durability test, the specimen is characterized by the presence of loops consisting of 3-5 graphene layers at the sidewalls of pCNF2400. After two weeks of polarization, those loops are completely opened. Therefore, in the case of pCNF2400, this loop edge structure can be considered the priority site for corrosion. The similar diameter of pCNF2400 nanofibers after the durability test for 2 weeks and 1 month (Figs. S5b and S5c, respectively) and the similar carbon edge structure at the sidewalls indicate that the oxidation of pCNF2400 at the exposed carbon edge planes is extremely slow, contributing to the high durability of pCNF2400 under OER conditions.

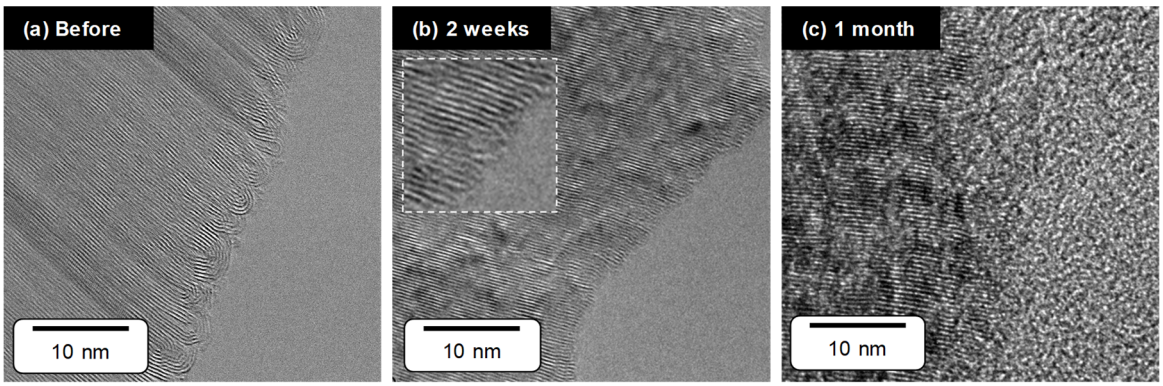

Fig. 8 High-resolution TEM images of pCNF2400 (a) before and (b, c) after the durability tests of the pCNF2400/CFCO electrode for (b) 2 weeks and (c) 1 month.

3.3 Factors influencing carbon corrosion

The durability tests provided under the OER conditions supported by *ex situ* observations of carbon degradation indicated that there are three key factors affecting carbon corrosion, *i.e.*, i) low or high graphitization degree, ii) exposure of basal planes, and iii) exposure of edge planes.

Both DB and DB2400 carbons have (i) poor graphitization degree and (ii) exposed basal planes. The combination of these two factors resulted in a very poor corrosion resistance towards OER. The first factor may be simply understood with reference to hexagonal carbon, which is the most thermodynamically stable form of carbon. All other forms of carbon, such as those of DB, are metastable. Since the DB has a very low degree of crystallinity among the studied carbons, less energy appears to be required to break the carbon-carbon bonds and consequently oxidize carbon to CO_3^{2-} according to reactions (2-4). This consideration is in line with observations by others that highly graphitized carbon possesses high oxidation resistance [23]. The second factor is related to the disorganized structure of the particle and therefore the exposure of basal planes to the electrolyte, which tend to be more susceptible to pitting-type corrosion.

One negative and one positive factor for carbon corrosion were observed for pCNF1500, *i.e.*, i) low graphitization degree and iii) exposed edge planes. Such a combination is not effective for

providing long-term durability, as pCNF1500 corroded with a similar rate to DB, which indicates that the low graphitization degree is not suitable to improve the durability. In contrast to pCNF1500, the MWCNT carbon has the opposite combination of crystallinity and edge structure, *i.e.*, i) high graphitization degree and ii) exposed basal planes. Relatively fast degradation of the carbon appears to originate from pitting-type corrosion on basal planes.

Among the studied structures, pCNF2400 is the most corrosion-resistant carbon material and provides long-term durability as a result of the combination of two positive factors: i) high graphitization degree and ii) exposed edge planes. The kinetics of carbon oxidation from the carbon edge planes are slower than those from the carbon basal planes due to a change in the corrosion mechanism from pitting-type to general-type corrosion. It is not completely understood how the edge planes suppress the rate of carbon oxidation; however, edge termination and/or passivation effects may be possible. We also note the one possibility that the priority adsorption of oxygen molecules on the carbon edge plane [27]. This adsorption has the possibility to disconnect the carbon and corrosion environment. Further, more in-depth *in situ* studies on this aspect are necessary. One of the most unique features for pCNF2400 is the loop-edge structure observed in Fig. 3b. The loop composed of 3-5 graphene layers, however, has only a slight influence on the corrosion performance of the carbon. The graphene layers forming the loop are possibly oxidized by a mechanism similar to that of MWCNTs in which corrosion-resistant edge planes are uncovered; therefore, the corrosion resistance is essentially provided by the carbon edge planes. It has been often discussed that carbon edge planes become preferential sites for the oxidation of carbon materials [24-27], but the present study discloses that the edge planes of carbon nanofibers with a high graphitization degree are more resistant to oxidation under OER conditions in highly alkaline electrolytes. The findings in this study show the high oxidation resistance of carbon edge planes in highly graphitized carbon nanofibers, opening a new avenue for designing durable air electrodes using carbon materials as a conductive support.

4. Conclusions

Carbon nanomaterials with various orientations of the carbon planes were studied as conductive supports in combination with a state-of-the-art brownmillerite CFCO electrocatalyst for OER/ORR in a 4 mol dm^{-3} KOH electrolyte. It was found that the appropriate arrangement of the exposed carbon planes with a relatively high degree of graphitization plays a key role in providing long-term durability of the carbon nanostructure in strongly alkaline electrolytes. Among the studied materials, the carbon nanofibers with graphene layers arranged perpendicularly to the fiber axis of the nanofibers, *i.e.*, carbon edge planes, were most durable under OER conditions without significant decay of the electrocatalytic activity for one month of testing. In contrast, the exposure of basal planes led to a change in the carbon degradation process from general-type to pitting-type corrosion with faster oxidation kinetics. The highly graphitized platelet-type carbon nanofibers are therefore promising as conductive carbon supports for durable air electrodes in rechargeable metal-air batteries using alkaline aqueous electrolytes.

Declaration of competing interest

The authors declare that they have no known competing financial interests or personal relationships that could have appeared to influence the work reported in this paper.

Acknowledgements

This work was supported in part by the RISING2 (Research and Development Initiative for Science Innovation of New Generation Batteries 2) of the New Energy and Industrial Technology Development Organization (NEDO), Japan. A part of this work was conducted at High-Voltage Electron Microscope Laboratory, Hokkaido University, supported by “Nanotechnology Platform” Program of the Ministry of Education, Culture, Sports, Science and Technology (MEXT), Japan. Y. S. would like to acknowledge for financial support from the Ministry of Education, Culture, Sports, Science and

Technology through Program for Leading Graduate Schools (Hokkaido University "Ambitious Leader's Program").

References

[1] Y. Zhu, W. Zhou, Z. Shao, Perovskite/Carbon Composites: Applications in Oxygen Electrocatalysis, Small, 13 (12) (2017) 1603793. https://doi.org/10.1002/smll.201603793

[2] E. Tsuji, A. Imanishi, K.I. Fukui, Y. Nakato, Electrocatalytic activity of amorphous RuO_2 electrode for oxygen evolution in an aqueous solution, Electrochim. Acta, 56 (5) (2011) 2009-2016. https://doi.org/10.1016/j.electacta.2010.11.062

[3] M. Yagi, E. Tomita, T. Kuwabara, Remarkably high activity of electrodeposited IrO_2 film for electrocatalytic water oxidation, J. Electroanal. Chem., 579 (1) (2005) 83-88. https://doi.org/10.1016/j.jelechem.2005.01.030

[4] A. A. Gewirth, M. S. Thorum, Electroreduction of Dioxygen for Fuel-Cell Applications: Materials and Challenges, Inorg. Chem., 49 (8) (2010) 3557-3566. https://doi.org/10.1021/ic9022486

[5] M. Risch, K. A. Stoerzinger, S. Maruyama, W.T. Hong, I. Takeuchi, Y. S. Horn, $La_{0.8}Sr_{0.2}MnO_{3-\delta}$ Decorated with $Ba_{0.5}Sr_{0.5}Co_{0.8}Fe_{0.2}O_{3-\delta}$: A Bifunctional Surface for Oxygen Electrocatalysis with Enhanced Stability and Activity, J. Am. Chem. Soc., 136 (14) (2014) 5229-5232. https://doi.org/10.1021/ja5009954

[6] Y. Aoki, E. Tsuji, T. Motohashi, D. Kowalski, H. Habazaki, $La_{0.7}Sr_{0.3}Mn_{1-x}Ni_xO_{3-\delta}$ Electrocatalysts for the Four-Electron Oxygen Reduction Reaction in Concentrated Alkaline Media, J. Phys. Chem. C, 122 (39) (2018) 22301-22308. https://doi.org/10.1021/acs.jpcc.8b06741

[7] Y. Miyahara, K. Miyazaki, T. Fukutsuka, T. Abe, Influence of Surface Orientation on the Catalytic Activities of $La_{0.8}Sr_{0.2}CoO_3$ Crystal Electrodes for Oxygen Reduction and Evolution Reactions,

ChemElectroChem, 3 (2) (2016) 214-217.
https://doi.org/10.1002/celc.201500439

[8] J. S. Sagu, D. Mehta, K. G. U. Wijayantha, Electrocatalytic activity of $CoFe_2O_4$ thin films prepared by AACVD towards the oxygen evolution reaction in alkaline media, Electrochem. Commun., 87 (2018) 1-4. https://doi.org/10.1016/j.elecom.2017.12.017

[9] M. Guo, K. Xu, Y. Qu, F. Zeng, C. Yuan, Porous Co_3O_4/CoS_2 nanosheet-assembled hierarchical microspheres as superior electrocatalyst towards oxygen evolution reaction, Electrochim. Acta, 268 (1) (2018) 10-19. https://doi.org/10.1016/j.electacta.2018.02.088

[10] E. Tsuji, T. Motohashi, H. Noda, D. Kowalski, Y. Aoki, H. Tanida, J. Nikura, Y. Koyama, M. Mori, H. Arai, T. Ioroi, N. Fujiwara, Y. Uchimoto, Z. Ogumi, H. Habazaki, Brownmillerite-type Ca_2FeCoO_5 as a Practicable Oxygen Evolution Reaction Catalyst, ChemSusChem., 10 (14) (2017) 2864-2868. https://doi.org/10.1002/cssc.201700499

[11] D. Kowalski, H. Kiuchi, T. Motohashi, Y. Aoki, H. Habazaki, Activation of Catalytically Active Edge-Sharing Domains in Ca_2FeCoO_5 for Oxygen Evolution Reaction in Highly Alkaline Media, ACS Appl. Mater. Interfaces, 11 (32) (2019) 28823-28829.
https://doi.org/10.1021/acsami.9b06854

[12] Y. Sato, Y. Aoki, K. Takase, H. Kiuchi, D. Kowalski, H. Habazaki, "A Highly Durable OER Catalyst: Amorphous Oxyhydroxide Derived from Brownmillerite-type Ca_2FeCoO_5", *ACS Applied Energy Materials,* under review.

[13] V. Cascos, R. Martínez-Coronado, J.A. Alonso, M.T. Fernández-Díaz, Structural and electrical characterization of the Co-doped $Ca_2Fe_2O_5$ brownmillerite: Evaluation as SOFC -cathode materials, International Journal of Hydrogen Energy, 40 (15) (2015) 5456-5468.
https://doi.org/10.1016/j.ijhydene.2015.01.067

[14] Li Q., Sun L., Huo L., Zhao H., Grenier J.-C., Electrode properties of Co-doped $Ca_2Fe_2O_5$ as new cathode materials for intermediate-temperature SOFCs, International Journal of Hydrogen Energy,

35 (17) (2010) 9151−9157. https://doi.org/10.1016/j.ijhydene.2010.06.048

[15] S. Thundiyil, Sr. Kurungot, R. Nandini Devi, Bifunctional Oxygen Reduction and Evolution Activity in Brownmillerites $Ca_2Fe_{(1-x)}Co_xO_5$, ACS Omega, 4 (1) (2019) 31−38 https://doi.org/10.1021/acsomega.8b02468

[16] R. Mohamed, X. Cheng, E. Fabbri, P. Levecque, R. Kotz, O. Conrad, T. J. Schmidt, Understanding the Influence of Carbon on the Oxygen Reduction and Evolution Activities of BSCF/Carbon Composite Electrodes in Alkaline Electrolyte, ECS Trans., 58 (36) (2014) 9-18. https://doi.org/10.1149/05836.0009ecst

[17] E. Fabbri, M. Nachtegaal, X. Cheng, T. J. Schmidt, Superior Bifunctional Electrocatalytic Activity of $Ba_{0.5}Sr_{0.5}Co_{0.8}Fe_{0.2}O_{3-\delta}$/Carbon Composite Electrodes: Insight into the Local Electronic Structure, Adv. Eng. Mater., 5 (17) (2015) 1402033. https://doi.org/10.1002/aenm.201402033

[18] D. G. Lee, O. Gwon, H. S. Park, S. H. Kim, J. Yang, S. K. Kwak, G. Kim, H. K. Song, Conductivity-Dependent Completion of Oxygen Reduction on Oxide Catalysts, Angew. Chem. Int. Ed., 54 (52) (2015) 15730-15733. https://doi.org/10.1002/anie.201508129

[19] K. Kinoshita, Electrochemical Oxygen Technology, New York: John Wiley & Sons (1992) pp. 289-300.

[20] K. Ono, T. Kinumoto, T. Tsumura, M. Toyoda, Preparation of $LaMnO_3$-CNF and Its Activity for Oxygen Electrode Reaction in 0.1 mol dm^{-3} KOH Solution, ECS Trans., 64 (45) (2015) 29-39. https://doi.org/10.1149/06445.0029ecst

[21] M. Pourbaix, Atlas of Electrochemical Equilibria in Aqueous Solutions, London: Pergamon Press Ltd. (1966) pp 449-457.

[22] M. Tominaga, Y. Yatsugi, N. Watanabe, Oxidative corrosion potential vs. pH diagram for single-walled carbon nanotubes, RSC Adv., 4 (2014) 27224-27227. https://doi.org/10.1039/C4RA02875A

[23] P. Ross and M. Sattler, The Corrosion of Carbon Black Anodes in Alkaline Electrolyte III. The Effect of Graphitization on the Corrosion Resistance of Furnace Blacks, J. Electrochem. Soc., 135 (6) (1988) 1464-1470. https://doi.org/10.1149/1.2096029

[24] Z. Shiroma. M. Tanaka, K. Yasuda, K. Tanimoto, M. Inaba. A. Tasaka, Electrochemical Corrosion of Carbon Materials in an Aqueous Acid Solution, Electrochemistry, 75 (2) (2007) 258-260. https://doi.org/10.5796/electrochemistry.75.258

[25] N. Staud, H. Sokol, P. N. Ross Jr., The Corrosion of Carbon Black Anodes in Alkaline Electrolyte IV. Current Efficiencies for Oxygen Evolution from Metal Oxide-Impregnated Graphitized Furnace Blacks, J. Electrochem. Soc., 136 (12) (1989) 3570-3576. https://doi.org/10.1149/1.2096511

[26] C. Lafforgue, A. Zadick, L. Dubau, F. Maillard, M. Chatenet, Selected Review of the Degradation of Pt and Pd-based Carbon-supported Electrocatalysts for Alkaline Fuel Cells: Towards Mechanisms of Degradation, Fuel Cells, 18 (3) (2018) 229-238. https://doi.org/10.1002/fuce.201700094

[27] L. Tao, Q. Wang, S. Dou, Z. Ma, J. Huo, S. Wang, L. Dai, Edge-rich and dopant-free graphene as a highly efficient metal-free electrocatalyst for the oxygen reduction reaction, Chem. Commun., 52 (2016) 2764–2767. https://doi.org/10.1039/C5CC09173J

[28] E. Tsuji, T. Yamasaki, Y. Aoki, S. G. Park, K. Shimizu, H. Habazaki, Highly durable platelet carbon nanofiber-supported platinum catalysts for the oxygen reduction reaction, Carbon, 87 (2105) 1-9. https://doi.org/10.1016/j.carbon.2015.01.027

[29] N. Yamada, D. Kowalski, C. Zhu, Y. Aoki, H. Habazaki, High dispersion and oxygen reduction reaction activity of Co_3O_4 nanoparticles on platelet-type carbon nanofibers, RSC Advances, 9 (2019) 3726-3733. https://doi.org/10.1039/C8RA09898K

[30] H. Habazaki, M. Kiriu, H. Konno, High rate capability of carbon nanofilaments with platelet structure as anode materials for lithium ion batteries, Electrochemistry Commun., 8 (8) (2006)

1275-1279. https://doi.org/10.1016/j.elecom.2006.06.012

[31] H. Habazaki, M. Kiriu, M. Hayashi, H. Konno, Structure of the carbon nanofilaments formed by liquid phase carbonization in porous anodic alumina template, Mater. Chem. Phys., 105 (2007) 367-372. https://doi.org/10.1016/j.matchemphys.2007.04.074

[32] S. Lim, S. H. Yoon, I. Mochida, J. H. Chi, Surface Modification of Carbon Nanofiber with High Degree of Graphitization, J. Phys. Chem. B, 108 (5) (2004) 1533-1536. https://doi.org/10.1021/jp036819r

[33] K. Moriguchi, S. Munetoh, M. Abe, M. Yonemura, K. Kamei, A. Shintani, Y. Maehara, A. Omaru, M. Nagamine, Nano-tube-like surface structure in graphite particles and its formation mechanism: A role in anodes of lithium-ion secondary batteries, Journal of Applied Physics, 88 (11) (2000) 6369. https://doi.org/10.1063/1.1322596

[34] S. H. Yoon, S. Lim, S. H. Hong, I. Mochida, B. An, K. Yokogawa, Carbon nano-rod as a structural unit of carbon nanofibers, Carbon, 42 (15) (2004) 3087-3095. https://doi.org/10.1016/j.carbon.2004.07.022

[35] J. Suntivich, H. A. Gasteiger, N. Yabuuchi, Y. S. Horn, Electrocatalytic Measurement Methodology of Oxide Catalysts Using a Thin-Film Rotating Disk Electrode, J. Electrochem. Soc., 157 (8) (2010) B1263-B1268. https://doi.org/10.1149/1.3456630

[36] M. Acik, Y. J. Chabal, Nature of Graphene Edges: A Review, Jpn. J. Appl. Phys, 50 (2011) 070101. https://doi.org/10.1143/JJAP.50.070101

[37] M. Velický, P. S. Toth, C. R. Woods, K. S. Novoselov, R. A. W. Dryfe, Electrochemistry of the Basal Plane versus Edge Plane of Graphite Revisited, J. Phys. Chem. C, 123 (18) (2019) 11677-11685. https://doi.org/10.1021/acs.jpcc.9b01010

[38] R. Hurt, G. Krammer, G. Crawford, K. Jian, C. Rulison, Polyaromatic Assembly Mechanisms and Structure Selection in Carbon Materials, Chem. Mater., 14 (11) (2002) 4558-4565. https://doi.org/10.1021/cm020310b

[39] K. K. Mani and R. Ramani, Lattice Dynamics of Graphite, Phys., Stat. Sol. (b), 61 (2) (1974) 659-668. https://doi.org/10.1002/pssb.2220610232

[40] Y. Kawashima and G. Katagiri, Observation of the out-of-plane mode in the Raman scattering from the graphite edge plane, Physical Review B, 59 (1) (1999) 62. https://doi.org/10.1103/PhysRevB.59.62

[41] F. Tuinstra and J. L. Koenig, Raman Spectrum of Graphite, J. Chem. Phys., 53 (1976) 1126. https://doi.org/10.1063/1.1674108

[42] M. S. Dresselhaus, A. Jorio, M. Hofmann, G. Dresselhaus, R. Saito, Perspectives on Carbon Nanotubes and Graphene Raman Spectroscopy, Nano Lett., 10 (3) (2010) 751. https://doi.org/10.1021/nl904286r

[43] A. Cuesta, P. Dhamelincourt, J. Laureyns, A. Martinezalonso, J. M. D. Tascon, Raman microprobe studies on carbon materials, Carbon, 32 (8) (1994) 1523-1532. https://doi.org/10.1016/0008-6223(94)90148-1

[44] S. Campisi, F. J. S. Trujillo, D. Motta, T. E. Davies, N. Dimitratos, A. Villa, Controlling the Incorporation of Phosphorus Functionalities on Carbon Nanofibers: Effects on the Catalytic Performance of Fructose Dehydration, C — Journal of Carbon Research —, 4 (1) (2018) 9. https://doi.org/10.3390/c4010009

[45] Y. Meng, W. Song, H. Huang, Z. Ren, S. Y. Chen, S. L. Sui Structure−Property Relationship of Bifunctional MnO_2 Nanostructures: Highly Efficient, Ultra-Stable Electrochemical Water Oxidation and Oxygen Reduction Reaction Catalysts Identified in Alkaline Media, J. Am. Chem. Soc., 136 (32) (2014) 11452-11464. https://doi.org/10.1021/ja505186m

[46] H. Antoni, D. M. Morales, J. Bitzer, Q. Fu, Y. T. Chen, J. Masa, W. Kleist, W. Schuhmann, Martin Muhler, Enhancing the water splitting performance of cryptomelane-type α-(K) MnO_2, J. Catal., 374 (2019) 335-344. https://doi.org/10.1016/j.jcat.2019.05.010

[47] Y. J. Min, S. J. Oh, M. S. Kim, J. H. Choi, S. Eom, Effect of carbon properties on the

electrochemical performance of carbon-based air electrodes for rechargeable zinc–air batteries, J. Appl. Electrochem., 48 (4) (2018) 405-413. https://doi.org/10.1007/s10800-018-1173-7

[48] P. J. Kulesza, J. K. Zak, I. A. Rutkowska, B. Dembinska, S. Zoladek, K. Miecznikowski, E. Negro, V. D. Noto, P. Zelenay, Elucidation of role of graphene in catalytic designs for electroreduction of oxygen, Current Opinion in Electrochemistry, 9 (2018) 257-264. https://doi.org/10.1016/j.coelec.2018.05.012

[49] X. Y. Yan, X. L. Tong, Y. F. Zhang, X. D. Han, Y. Y. Wang, G. Q. Jin, Y. Qina, X. Y. Guo, Cuprous oxide nanoparticles dispersed on reduced graphene oxide as an efficient electrocatalyst for oxygen reduction reaction, Chem. Commun., 48 (2012). 1892-1894. https://doi.org/10.1039/C2CC17537A

[50] H. Tang, H. Yin, J. Wang, N. Yang, D. Wang, Z. Tang, Molecular Architecture of Cobalt Porphyrin Multilayers on Reduced Graphene Oxide Sheets for High-Performance Oxygen Reduction Reaction, Angew. Chem. Int. Ed., 52 (21) (2013) 5585-5589. https://doi.org/10.1002/anie.201300711

[51] J. Zhou, Y. Wang, X. Su, S. Gu, R. Liu, Y. Huang, S. Yan, J. Li, S. Zhang, Electrochemically accessing ultrathin Co (oxy)-hydroxide nanosheets and operando identifying their active phase for the oxygen evolution reaction, Energy Environ. Sci., 12 (2019) 739-746. https://doi.org/10.1039/C8EE03208D

[52] M. W. Kanan and D. G. Nocera, In situ formation of an oxygen-evolving catalyst in neutral water containing phosphate and Co^{2+}, Science, 321 (5982) (2008) 1072-1075. https://doi.org/10.1126/science.1162018

[53] M. Yoshida, T. Mineo. Y. Mitsutomi, F. Yamamoto, H. Kurosu, S. Takakusagi, K. Asakura, H. Kondoh, Structural Relationship between CoO_6 Cluster and Phosphate Species in a Cobalt - Phosphate Water Oxidation Catalyst Investigated by Co and P K-edge XAFS, Chem. Lett, 45 (3) (2016) 277-279. https://doi.org/10.1246/cl.151073

[54] M. Risch, A. Grimaud, K. J. May, K. A. Stoerzinger, T. J. Chen, A. N. Mansour, Y. S. Horn, Structural Changes of Cobalt-Based Perovskites upon Water Oxidation Investigated by EXAFS, J. Phys. Chem. C, 117 (17) (2013) 8628-8635. https://doi.org/10.1021/jp3126768

[55] S. H. Ye, Z. X. Shi, J. X. Feng, Y. X. Tong, G. R. Li, Activating CoOOH Porous Nanosheet Arrays by Partial Iron Substitution for Efficient Oxygen Evolution Reaction, Angew. Chem. Int. Ed., 57 (10) (2018) 2672-2676. https://doi.org/10.1002/anie.201712549

[56] E. L. Evans, R. J. M. Griffiths, J. M. Thomas, Kinetics of Single-Layer Graphite Oxidation: Evaluation by Electron Microscopy, Science, 171 (3967) (1971) 174-175. https://doi.org/10.1126/science.171.3967.174

[57] A. Tracz, G. Wegner, J. P. Rabe Kinetics of surface roughening via pit growth during the oxidation of the basal plane of graphite. 1. Experiments, Langmuir, 9 (11) (1993) 3033-3038. https://doi.org/10.1021/la00035a048

[58] Y. Yi, J. Tornow, E. Willinger, M. G. Willinger, C. Ranjan, R. Schlögl, Electrochemical Degradation of Multiwall Carbon Nanotubes at High Anodic Potential for Oxygen Evolution in Acidic Media, ChemElectroChem, 2 (12) (2015) 1929-1937. https://doi.org/10.1002/celc.201500268